Numerical experiments with model equations of cancer invasion of tissue

Abstract

In this paper we investigate a mathematical model of cancer invasion of tissue, which incorporates haptotaxis, chemotaxis, proliferation and degradation rates for cancer cells and the extracellular matrix, kinetics of urokinase receptor, and urokinase plasminogen activator cycle. We solve the model using spectrally accurate approximations and compare its numerical solutions with laboratory data. The spectral accuracy allows to use low-dimensional matrices and vectors, which speeds up the computations of the numerical solutions and thus to estimate the parameter values for the model equations. Our numerical results demonstrate correlations between numerical data computed from the mathematical model and *in vivo* tumour growth rates from prostate cell lines.

Keywords: *In Vivo* Tumorigenicity; Cancer Cells; Proliferation; Chemotaxis; Haptotaxis; Extracellular Matrix; Tumour Invasion; Mathematical Model; Animal Models; Approximations.

*Department of Mathematics and Computer Sciences, University of Warmia and Mazury, Olsztyn, Żolnierska 14, 10-561, Poland, e-mail: kolev@matman.uwm.edu.pl

†Department of Mathematics, Boise State University, 1910 University Drive, Boise, Idaho 83725, USA, e-mail: zubik@math.boisestate.edu, tel:(001)208-426-2802, fax:(001)208-426-1356

1 Introduction

Animal models prove useful to researchers in the manipulation of specific aspects of cancerogenic systems and for the testing of experimental therapies [12]. On the other hand, mathematical models demonstrate potential to provide alternatives to animal models and decrease the numbers of laboratory experiments and partially replace them by numerical experiments, which describe the behaviour of simulated tumours.

The purpose of the paper is to use the laboratory data [7] and compute parameter values for the mathematical model of cancer invasion of tissue, which includes differential equations for kinetics of urokinase receptor and urokinase plasminogen activator cycle, and incorporates haptotaxis, chemotaxis, and proliferation and degradation rates for cancer cells and the extracellular matrix [9]. We estimate the parameter values for the model equations by minimizing the error between the computed solutions and the available laboratory data.

In [13], the laboratory data [7] were successfully applied to estimate parameter values for the kinetic model [14], which is composed of partial integro-differential equations. The application of models of this type to tumour growth has been initiated by Bellomo and Forni [4] and developed later in a series of papers e.g., [3, 5, 10, 11]. Recently, Lachowicz [16] has proved that, for certain parameter ranges, a particular kinetic model considered on infinite domains is equivalent to the macroscopic model [8]. The result by Lachowicz [16] was a motivation for the parameter estimation in [15] for the model by Chaplain and Anderson [8]. Since the model [8] does not include differential equations describing kinetics of urokinase receptor and urokinase plasminogen activator cycle, in this paper, we apply the laboratory data [7] to the macroscopic model [9], which is different than the models in [8] and [14]. The parameter values for the macroscopic model [9], with differential equations describing kinetics of urokinase receptor and urokinase plasminogen activator cycle, were not yet estimated according to laboratory data.

For the estimation of the parameter values for the model [9], we construct a numerical algorithm based on spectrally accurate approximations. The approximations allow to use low-dimensional vectors of data for solving the model and save computational time for each solution computed for the selection of the parameter values.

The paper is organized as follows. A mathematical description of the model equations is provided in Section 2. In Section 3, we introduce the nu-

merical algorithm and present numerical experiments that lead to parameter estimation for the model equations and comparison of the resulting numerical solutions with the laboratory data. Finally, Section 4 includes our concluding remarks and future directions.

2 Oscillatory behaviour in the cancer cells and extracellular matrix proliferation terms

In this paper, we apply laboratory data and find parameter values for the mathematical model, which was introduced by Chaplain and Lolas [9]. For the cancer cell motion, they considered the following partial differential equation:

$$\frac{\partial n}{\partial t} = \underbrace{\frac{\partial}{\partial x}\Big(d_n \frac{\partial n}{\partial x}\Big)}_{dispersion} - \underbrace{\frac{\partial}{\partial x}\Big(\chi n \frac{\partial m}{\partial x}\Big)}_{chemotaxis} - \underbrace{\frac{\partial}{\partial x}\Big(\gamma n \frac{\partial f}{\partial x}\Big)}_{haptotaxis} + \underbrace{\mu_1 np(1-n-f)}_{proliferation}, \qquad (2.1)$$

where the tumour cell density n depends on time t and the spatial variable x from the scaled domain $[0,1]$. Moreover, d_n is the random motility coefficient, μ_1 is the proliferation rate of the tumour cells, and χ and γ are the chemotactic and haptotactic coefficients, respectively. The proliferation of tumour cells is modelled by the term $\mu_1 pn(1-n-f)$, which because of p, the concentration of the urokinase plasminogen activator (uPA) bound to the uPA receptor (uPAR), allows to incorporate the oscillatory behaviour in the cancer cells, cf. [9]. The unknown functions f and m represent the density of the extracellular matrix (ECM) and uPA concentration, respectively.

The extracellular matrix is a complex meshwork of proteins and proteoglycans that isolates tissue compartments, within which solid organs are placed [17]. The equation governing the processes of the ECM degradation and production is the following ordinary differential equation:

$$\frac{\partial f}{\partial t} = - \underbrace{\eta m f}_{proteolysis} + \underbrace{\mu_2 fp(1-n-f)}_{renewal}, \qquad (2.2)$$

where η and μ_2 are the rate constants for the degradation and growth, respectively. Motivated by the information on clinical observations of the increased production (re-establishment) of ECM in case of prostate cancer [17], we consider the model with $\mu_2 \neq 0$.

Proteases such as metalloproteases and serine proteases are enzymes that are released from tumours. They play very significant role in the degradation of ECM thus allowing the migration of cancer cells and their metastasis. The serine proteases of the plasminogen activation system includes urokinase uPA, which uses a specific uPA receptor (uPAR) to migrate through the ECM [1, 2]. The uPA is produced by the tumour cells, diffuses throughout the tissue, and undergoes decay. Therefore, the equation governing the evolution of uPA concentration is given by

$$\frac{\partial m}{\partial t} = \underbrace{d_m \frac{\partial^2 m}{\partial x^2}}_{diffusion} + \underbrace{\alpha n}_{production} - \underbrace{\beta m}_{decay}, \tag{2.3}$$

with constant diffusion coefficient d_m, production rate α, and decay rate β.

As in [9], we choose the following system of ordinary differential equations for the uPAR kinetics:

$$\begin{aligned} \frac{dp}{dt} &= q - 3 \\ \frac{dq}{dt} &= (q-3)\Big(1 - (p-2.1)^2\Big) - (p - 2.1), \end{aligned} \tag{2.4}$$

where q represents the concentration of the uPAR. Figure 18, [9], illustrates the limit cycle kinetics of the system (2.4). The combined system (2.1)-(2.4) overcomes the weakness of the models, which incorporate only constant reduction terms for cancer cells.

The system (2.1)-(2.4) is not complete and has to be closed by initial and boundary conditions. As in [8] and [9], we assume that at time $t = 0$, the initial small lump of cancer cells is centered around $x = 0$ and the function n has the initial distribution

$$n(x, 0) = \exp\,(-x^2/\epsilon), \tag{2.5}$$

with a positive constant ϵ. For the initial distribution of ECM and uPA we choose

$$f(x, 0) = 1 - 0.5n(x, 0), \quad m(x, 0) = 0.5n(x, 0), \tag{2.6}$$

where $x \in [0, 1]$, cf. [8], and we choose $p(0)$ and $q(0)$ according to numerical experiments and laboratory data. For the boundary conditions we choose the zero-flux conditions

$$\frac{\partial n}{\partial x}(0, t) = \frac{\chi}{d_n} n(0, t) \frac{\partial m}{\partial x}(0, t) + \frac{\gamma}{d_n} n(0, t) \frac{\partial f}{\partial x}(0, t), \qquad \frac{\partial m}{\partial x}(0, t) = 0 \tag{2.7}$$

at the left edge $x = 0$ and the Dirichlet conditions

$$n(1,t) = 0, \qquad m(1,t) = 0, \tag{2.8}$$

at the right edge $x = 1$ of the considered part of the tissue, which abuts a healthy part of the organism at $x = 1$.

The purpose of this paper is to apply the experimental data from [7] to the model (2.1)-(2.8) and demonstrate that its solutions correlate with the *in vivo* growths of prostate tumours tested in five nude mice [7]. In the next section, we construct a numerical algorithm for the model (2.1)-(2.8) and compute its parameters $\mu_1, \mu_2, \alpha, \beta, \gamma, \eta, \chi, d_n, d_m$ by minimizing the error between its numerical solutions and the experimental data from [7]. Since the solutions have to be computed for many different sets of the parameters, we construct the algorithm by using spectrally accurate approximations so that the resulting schemes are based on small amounts of spatial grid-points and low-dimensional vectors, which saves computational time for each solution corresponding to one combination of the parameters.

3 Numerical algorithm

Consider the Chebyshev-Gauss-Lobatto points

$$x_i = \frac{1}{2} - \frac{1}{2}\cos\frac{i\pi}{N+1}, \tag{3.1}$$

with $i = 0, 1, \ldots, N+1$ and the first order differentiation matrix

$$D = \left[d_{i,j}\right]_{i,j=0}^{N+1}$$

based on (3.1), see [6]. We use the following notations

$$n(t) = \begin{bmatrix} n(x_0,t) \\ n(x_1,t) \\ \vdots \\ n(x_N,t) \end{bmatrix}, \quad n_x(t) = \begin{bmatrix} \dfrac{\partial n}{\partial x}(x_0,t) \\ \dfrac{\partial n}{\partial x}(x_1,t) \\ \vdots \\ \dfrac{\partial n}{\partial x}(x_N,t) \end{bmatrix}, \quad n_{xx}(t) = \begin{bmatrix} \dfrac{\partial^2 n}{\partial x^2}(x_0,t) \\ \dfrac{\partial^2 n}{\partial x^2}(x_1,t) \\ \vdots \\ \dfrac{\partial^2 n}{\partial x^2}(x_N,t) \end{bmatrix},$$

and similar notations for f and m. For the first order derivatives, we obtain the following approximations

$$n_x(t) \approx D_0^{(1)} n(t) + \frac{\gamma}{d_n} n(x_0, t) s_0^f(t) e_1, \tag{3.2}$$

$$f_x(t) \approx D^{(1)} f(t) + f(x_{N+1}, t) w, \tag{3.3}$$

$$m_x(t) \approx D_0^{(1)} m(t), \tag{3.4}$$

with

$$D^{(1)} = \Big[d_{i,j} \Big]_{i,j=0}^{N},$$

and $D_0^{(1)}$ being an $N+1$ by $N+1$ matrix with zeros in the first row and the other rows as in $D^{(1)}$, w is an $N+1$ by 1 column vector including the entries of the last column of D except the last entry $d_{N+1,N+1}$, e_1 is the unit $N+1$ by 1 column vector and

$$s_0^f(t) = \sum_{j=0}^{N+1} d_{0,j} f(x_j, t).$$

From (3.4), we obtain the approximation

$$\begin{bmatrix} \frac{\partial}{\partial x}\Big(n(x_0,t)\frac{\partial m}{\partial x}(x_0,t)\Big) \\ \frac{\partial}{\partial x}\Big(n(x_1,t)\frac{\partial m}{\partial x}(x_1,t)\Big) \\ \vdots \\ \frac{\partial}{\partial x}\Big(n(x_N,t)\frac{\partial m}{\partial x}(x_N,t)\Big) \end{bmatrix} \approx D^{(1)}\Big(n(t) \odot \big(D^{(1)} m(t) \big) \Big),$$

for the chemotaxis term in (2.1). Here, $\odot$ stands for the component-wise multiplication between two vectors. From (3.3) we obtain

$$\begin{bmatrix} \frac{\partial}{\partial x}\Big(n(x_0,t)\frac{\partial f}{\partial x}(x_0,t)\Big) \\ \frac{\partial}{\partial x}\Big(n(x_1,t)\frac{\partial f}{\partial x}(x_1,t)\Big) \\ \vdots \\ \frac{\partial}{\partial x}\Big(n(x_N,t)\frac{\partial f}{\partial x}(x_N,t)\Big) \end{bmatrix} \approx D^{(1)}\Big(n(t) \odot \big(D^{(1)} f(t) + f(x_{N+1},t) w \big) \Big),$$

for the haptotactic term. Considering the general case with the random motility coefficient $d_n = d_n(f, m)$, which may be a function of ECM or/and uPA, for the dispersion term in (2.1), from (3.2), we obtain the approximation

$$\begin{bmatrix} \frac{\partial}{\partial x}\Big(d_{n,0}(t)\frac{\partial n}{\partial x}(x_0,t)\Big) \\ \frac{\partial}{\partial x}\Big(d_{n,1}(t)\frac{\partial n}{\partial x}(x_1,t)\Big) \\ \vdots \\ \frac{\partial}{\partial x}\Big(d_{n,N}(t)\frac{\partial n}{\partial x}(x_N,t)\Big) \end{bmatrix} \approx \begin{array}{c} D^{(1)}\bigg(d_n(t)\odot\Big(D_0^{(1)}n(t)+\frac{\gamma}{d_n}n(x_0,t)s_0^f(t)e_1\Big)\bigg) \\ +d_{n,N}(t)s_{N+1}^n(t)w, \end{array}$$

where

$$d_n(t) = \begin{bmatrix} d_{n,0}(t) \\ d_{n,1}(t) \\ \vdots \\ d_{n,N}(t) \end{bmatrix}, \quad d_{n,i}(t) = d_n(x_i,t),\ i = 0,1,\ldots,N.$$

and

$$s_{N+1}^n(t) = \sum_{j=0}^{N+1} d_{N+1,j}n(x_j,t).$$

From (2.1) and the above three approximations, for the chemotaxis, haptotaxis, and dispersion terms, we obtain the following ordinary differential equation

$$\begin{aligned} \frac{dn}{dt}(t) &= D^{(1)}\bigg(d_n(t)\odot\Big(D_0^{(1)}n(t)+\frac{\gamma}{d_n}n(x_0,t)s_0^f(t)e_1\Big)\bigg) \\ &+ d_{n,N}(t)s_{N+1}^n(t)w - \chi D^{(1)}\bigg(n(t)\odot\Big(D^{(1)}m(t)\Big)\bigg) \\ &- \gamma D^{(1)}\bigg(n(t)\odot\Big(D^{(1)}f(t)+f(x_{N+1},t)w\Big)\bigg) \\ &+ \mu_1 n(t)\odot p(t)\odot\Big(1-n(t)-f(t)\Big). \end{aligned} \tag{3.5}$$

The discrete form for (2.2) is written in the following way

$$\frac{df}{dt}(t) = f(t)\odot\bigg(\mu_2 p(t)\odot\Big(1-n(t)-f(t)\Big)-\eta m(t)\bigg). \tag{3.6}$$

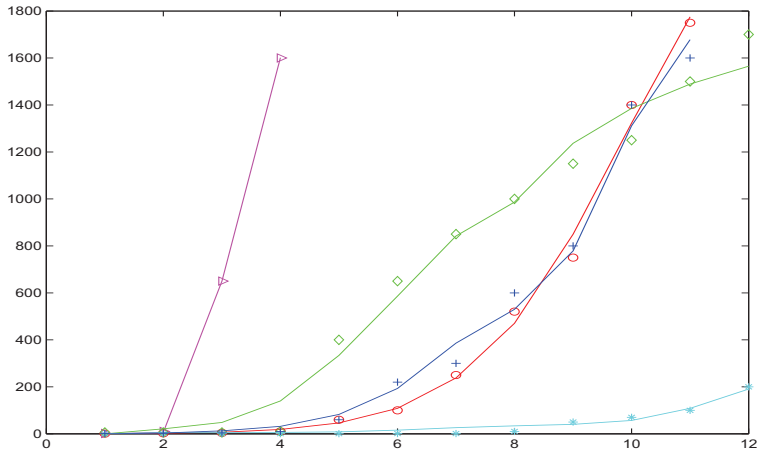

Figure 1: Laboratory versus numerical data.

The diffusion of the uPA can be approximated by

$$m_{xx}(t) \approx D^{(1)} m_x(t) + s^m_{N+1}(t) w,$$

which, from (3.4), gives

$$m_{xx}(t) \approx D^{(1)} D^{(1)}_0 m(t) + s^m_{N+1}(t) w$$

and results in the following discrete form for (2.3)

$$\frac{dm}{dt}(t) = d_m D^{(1)} D^{(1)}_0 m(t) + d_m s^m_{N+1}(t) w + \alpha n(t) - \beta m(t). \tag{3.7}$$

The system of ordinary differential equations (3.5), (3.6), (3.7), and (2.4) is not completed and has to be closed by initial conditions. From (2.5)-(2.6) we obtain

$$n(0) = \begin{bmatrix} \exp\left(-x_0^2/\epsilon\right) \\ \exp\left(-x_1^2/\epsilon\right) \\ \vdots \\ \exp\left(-x_N^2/\epsilon\right) \end{bmatrix} \tag{3.8}$$

and the starting vectors for the ECM and uPA are

$$f(0) = 1 - 0.5n(0), \quad m(0) = 0.5n(0), \tag{3.9}$$

respectively. The initial conditions

$$p(0) = 1, \quad q(0) = 1$$

are chosen according to the numerical experiments with the semi-discrete scheme (3.5), (3.6), (3.7), (2.4), (3.8), and (3.9) and comparison of the numerical results with the laboratory data [7].

The parameter values $\mu_1, \mu_2, \alpha, \beta, \gamma, \eta, \chi, d_n$, and d_m used in the model equations (2.1)-(2.3) and in the construction of the numerical scheme (3.5), (3.6), (3.7) are unknown and have to be estimated in order to find the approximations to the tumour cell density n, the ECM density f, and the uPA concentration m. In this paper, we apply the laboratory data [7] to estimate the parameter values for the model (2.1)-(2.3).

The laboratory data [7] are displayed in Figure 1 by $\triangleright$, $\diamond$, $+$, $\circ$, and $*$ for the *in vivo* tumour growth rates from the five prostate Pr14C1, Pr14C2, Pr117, Pr14, and Pr111 cell lines, respectively. For comparison, the numerical data are displayed by the solid curves. The laboratory data [7] are compared with numerical data computed from the model equations (2.1)-(2.4) with various sets of values assigned for the constants $\mu_1, \mu_2, \alpha, \beta, \gamma, \eta, \chi, d_n$, and d_m. Each set of the constants gives a different solution n and among many solutions, for each prostate cell line, only the solutions which capture the main characteristic features of the *in vivo* tumour growth rates are chosen. This selection of solutions of the model equations (2.1)-(2.4) and their corresponding parameter values is computationally expensive and thus the design of the numerical algorithm is crucial in the estimations of the unknown parameters. Since our algorithm is based on spectrally accurate approximations for the partial derivatives with respect to x, instead of using large dimensional vectors, like e.g. in finite difference schemes, we use low dimensional vectors and save computational time for each solution computed for the selection of the parameter values.

For each cell line, the parameter values are chosen according to the minimal error between the data and the computed values $v(t) = \frac{4}{3}\pi r^3(t)$, where

$$r(t) = k \int_0^1 n(x,t)dx,$$

and k is a constant of proportionality approximated by using the vertical scale in Fig. 1I, [7]. Here,

$$\int_0^1 n(x,t)dx \in [0,1]$$

corresponds with a mass of cells along a line segment scaled to the x-domain $[0, 1]$, which is shifted in such a way that the tumours are centered around $x = 0$. The resulting parameter values are listed for each cell line in Table 1 and the solutions that correspond to these parameter values are presented in Figure 1.

Param.	Pr111	Pr117	Pr14	Pr14C2	Pr14C1
μ_1	$5.1 \cdot 10^{-1}$	$1.4 \cdot 10^{1}$	$4.6 \cdot 10^{2}$	$1.3 \cdot 10^{5}$	9.0
μ_2	$2.9 \cdot 10^{-4}$	$7.7 \cdot 10^{-9}$	$1.3 \cdot 10^{-14}$	$8.9 \cdot 10^{1}$	$2.9 \cdot 10^{-3}$
α	2.9	$7.8 \cdot 10^{-1}$	2.9	1.1	5.8
β	$3.5 \cdot 10^{-3}$	$8.4 \cdot 10^{-6}$	$3.7 \cdot 10^{-5}$	$9.1 \cdot 10^{-9}$	$3.8 \cdot 10^{-10}$
γ	$7.8 \cdot 10^{-3}$	$3.2 \cdot 10^{-9}$	$1.7 \cdot 10^{-9}$	$1.6 \cdot 10^{1}$	$3.7 \cdot 10^{-10}$
χ	$8.2 \cdot 10^{-11}$	$2.2 \cdot 10^{-3}$	$1.0 \cdot 10^{-7}$	$1.0 \cdot 10^{-4}$	$6.6 \cdot 10^{-4}$
η	$4.9 \cdot 10^{-2}$	$5.4 \cdot 10^{-1}$	$2.4 \cdot 10^{-1}$	$3.6 \cdot 10^{-1}$	2.0
d_n	$6.4 \cdot 10^{-3}$	$6.5 \cdot 10^{-2}$	$7.0 \cdot 10^{-2}$	$1.2 \cdot 10^{2}$	$2.8 \cdot 10^{-1}$
d_m	$8.7 \cdot 10^{-8}$	$1.9 \cdot 10^{-16}$	$3.2 \cdot 10^{-12}$	$2.2 \cdot 10^{-15}$	$1.5 \cdot 10^{-10}$

Table 1: Parameter values for *in vivo* cell growth in C3(1)Tag Mice.

4 Concluding remarks and future directions

In this paper, we have applied the laboratory data [7] and have estimated parameter values for the mathematical model of cancer cell invasion of tissue, which includes the chemotaxis, haptotaxis, and proliferation terms [9]. The ability of the model to fit well the experimental data demonstrated in our paper confirms the usefulness of the mathematical modeling approach and the computational simulations in cancer research. In our future work we plan to develop the model for further investigations of mechanisms of cancer invasion and metastasis, which could be used for the design and improvement of treatment strategies.

References

[1] Andreasen PA, Kjoller L, Christensen L, Duffy MJ, The urokinase-type plasminogen activator system in cancer metastasis: A review, *International Journal of Cancer*, **72**, 1–22, 1997.

[2] Andreasen PA, Egelund R, Petersen HH, The plasminogen activation system in tumor growth, invasion, and metastasis, *Cellular and Molecular Life Sciences*, **57**, 25–40, 2000.

[3] Bellomo N, Delitala M, From the mathematical kinetic, and stochastic game theory to modelling mutations, onset, progression and immune competition of cancer cells, *Physics of Life Reviews*, **5**, 183–206, 2008.

[4] Bellomo N, Forni G, Dynamics of tumor interaction with the host immune system. *Math. Comput. Modelling,* **20**, 107–122, 1994.

[5] Bellomo N, Li NK, Maini PK, On the foundations of cancer modelling: Selected topics, speculations, and perspectives, *Math. Models Methods Appl. Sci.*, **18**, 593–646, 2008.

[6] Canuto C, Hussaini MY, Quarteroni A, Zang TA, Spectral Methods in Fluid Dynamics, Springer Verlag, New York, 1988.

[7] Calvo A, Xiao N, Kang J, Best CJM, Leiva I, Emmert-Buck MR, Jorcyk C, Green JE, Alterations in gene expression profiles during prostate cancer progression: functional correletions to tumorigenicity and down-regulation of selenoprotein-P in mouse and human tumors. *Cancer Research,* **62**, 5325–5335, 2002.

[8] Chaplain MAJ, Anderson ARA, Mathematical modelling of tissue invasion. Cancer modelling and simulation, 269–297, Chapman & Hall/CRC Math. Biol. Med. Ser., Chapman & Hall/CRC, Boca Raton, FL, 2003.

[9] Chaplain MAJ, Lolas G, Mathematical modelling of cancer invasion of tissue: dynamic heterogeneity, *Netw. Heterog. Media,* **1** (3), 399–439, 2006.

[10] De Angelis E, Lodz B, On the kinetic theory for active particles: A model for tumor-immune system competition. *Math. Comput. Modelling,* **47** (1-2), 196–209, 2008.

[11] De Lillo S, Salvatori MC, Bellomo N, Mathematical tools of the kinetic theory of active particles with some reasoning on the modelling progression and heterogeneity. *Math. Comput. Modelling,* **45** (5-6), 564–578, 2007.

[12] Holzer RG, MacDougall C, Cortright G, Atwood K, Green JE, Jorcyk CL, Development and characterization of a progressive series of mammary adenocarcinoma cell lines derived from the C3(1)/SV40 large T-antigen transgenic mouse model. *Breast Cancer Research Treat*, **77**, 65-76, 2003.

[13] Jackiewicz Z, Jorcyk CL, Kolev M, Zubik-Kowal B, Correlation between animal and mathematical models for prostate cancer progression, *Comput. Math. Methods Med.*, **10** (4), 241–252, 2009.

[14] Kolev M, A mathematical model of cellular immune response to leukemia. *Math. Comput. Modelling,* **41**, (2005), 1071-1081.

[15] Kolev M, Zubik-Kowal B, Numerical solutions for a model of tissue invasion and migration of tumour cells, in progress.

[16] Lachowicz M, Micro and meso scales of description corresponding to a model of tissue invasion by solid tumours. *Math. Models Methods Appl. Sci.*, **15** (11), 1667–1683, 2005.

[17] Liotta LA, Rao CN, Barsky SH, Tumour invasion and the extracellular matrix. *Lab. Invest.,* **49**, 636–649, 1983.